HHS Public Access

Author manuscript

Nat Phys. Author manuscript; available in PMC 2018 July 01.

Published in final edited form as:

Nat Phys. 2018 ; 14: 91–98. doi:10.1038/nphys4268.

Role of Graph Architecture in Controlling Dynamical Networks with Applications to Neural Systems

Jason Z. Kim,
Department of Bioengineering, University of Pennsylvania, Philadelphia, PA, 19104

Jonathan M. Soffer,
Department of Bioengineering, University of Pennsylvania, Philadelphia, PA, 19104

Ari E. Kahn,
Department of Neuroscience, University of Pennsylvania, Philadelphia, PA, 19104 and U.S. Army Research Laboratory, Aberdeen, MD 21001

Jean M. Vettel,
Human Research & Engineering Directorate, U.S. Army Research Laboratory, Aberdeen, MD 21001, Department of Bioengineering, University of Pennsylvania, Philadelphia, PA, 19104

Department of Psychological and Brain Sciences, University of California, Santa Barbara, CA, 93106

Fabio Pasqualetti, and
Department of Mechanical Engineering, University of California, Riverside, Riverside, CA, 92521

Danielle S. Bassett
Department of Bioengineering, University of Pennsylvania, Philadelphia, PA, 19104

Department of Electrical and Systems Engineering, University of Pennsylvania, Philadelphia, PA, 19104

Abstract

Networked systems display complex patterns of interactions between components. In physical networks, these interactions often occur along structural connections that link components in a hard-wired connection topology, supporting a variety of system-wide dynamical behaviors such as synchronization. While descriptions of these behaviors are important, they are only a first step towards understanding and harnessing the relationship between network topology and system behavior. Here, we use linear network control theory to derive accurate closed-form expressions that relate the connectivity of a subset of structural connections (those linking driver nodes to non-driver nodes) to the minimum energy required to control networked systems. To illustrate the utility of the mathematics, we apply this approach to high-resolution connectomes recently reconstructed from Drosophila, mouse, and human brains. We use these principles to suggest an

To whom correspondence should be addressed: dsb@seas.upenn.edu.

IX. STATEMENT OF INDIVIDUAL CONTRIBUTION

JZK, DSB, and FP wrote and revised the bulk of the manuscript. JZK developed the mathematical framework and analyzed the data with feedback from FP and DSB. JMS collected the human diffusion data, and AEK processed the data to produce structural connectivity matrices with support from JMV.

advantage of the human brain in supporting diverse network dynamics with small energetic costs while remaining robust to perturbations, and to perform clinically accessible targeted manipulation of the brain's control performance by removing single edges in the network. Generally, our results ground the expectation of a control system's behavior in its network architecture, and directly inspire new directions in network analysis and design via distributed control.

Network systems are composed of interconnected units that interact with each other on diverse temporal and spatial scales [1]. The exact patterns of interconnections between these units can take on many different forms that dictate how the system functions [2]. Indeed, specific features of network topology – such as small-worldness [3] and modularity [4] – can improve efficiency and robustness. Yet, exact mechanisms driving the relationship between structure and function remain elusive, hampering the analysis, modification, and control of interconnected complex systems. The relationship between interconnection architecture and dynamics is particularly important in biological systems such as the brain [5], where it is thought to support optimal information processing at cellular [6] and regional [7, 8] levels. Understanding structure-function relationships in this system could inform personalized therapeutics [9] including more targeted treatments for drug-resistant epilepsy to make the epileptic state energetically unfavorable to maintain [10, 11], especially due to the development of multi-site stimulation tools [12, 13] that allow for exponentially increasing stimulation configurations.

Existing paradigms seeking to explain how a complex network topology drives observable dynamics have advantages and disadvantages. Efforts in nonlinear dynamics define basins of attraction and perturbations driving a system between basins [14, 15]. Efforts in network science define graph metrics and report statistical correlations with observed functions such as attention [16] and learning [17, 18]. Neither approach offers comprehensive analytical solutions explaining mechanisms of control. A promising paradigm that meets these challenges is linear network control theory [19, 20], which assumes that the state of a system at a given time is a function of the previous state, the structural network linking system units, and injected control energy. From this paradigm, one can identify (i) driver nodes [21, 22] capable of influencing the system along diverse trajectories, and (ii) optimal inputs that move the system from one state to another with minimal cost. This latter formulation has proven useful in understanding the human brain where control points enable diverse cognitive strategies [23, 24], facilitate efficient intrinsic activation [25], and inform optimal targets for brain stimulation [26].

While practical tools exist, basic intuitions about the network properties that enhance control have remained elusive. Here, we address this challenge by formulating a linear control problem on the bipartite subgraph linking driver nodes to non-driver nodes, which provides excellent estimates of the control of the full network. Our results include analytical derivations of expressions relating a network's minimum control energy to its connectivity, an intuitive geometric representation to visualize this relationship, and rules for modifying edges to alter control energy in a predictable manner. While our mathematical contributions are applicable to any complex network system whose dynamics can be approximated by a linear model, we illustrate their utility in the context of networks estimated from the mouse

[27, 28], Drosophila [29], and human brain (Fig. 1d–f). Our results offer fundamental insights into the patterns of connections between brain regions that directly impact their minimum control energy, providing a link between the structure and function of neural systems and informing potential clinical interventions. An extension of this framework to non-bipartite graphs with corresponding results can be found in the supplementary methods and results.

I. NETWORK TOPOLOGY AND CONTROLLABILITY

We consider a network represented by the directed graph $\mathscr{G}=(\mathscr{V},\mathscr{E})$, where $\mathscr{V}=\{1,\ldots,n\}$ and $\mathscr{E}\subseteq\mathscr{V}\times\mathscr{V}$ are the sets of network vertices and edges, respectively. Let $a_{ij}\in\mathbb{R}$ be the weight associated with the edge $(i,j)\in\mathscr{E}$, and let $A=[a_{ij}]$ be the weighted adjacency matrix of $\mathscr{G}$. We associate a real value (*state*) with each node, collect the nodes' states into a vector (*network state*), and define the map $\boldsymbol{x}:\mathbb{R}_{\geq 0}\rightarrow\mathbb{R}^n$ to describe the evolution (*dynamics*) of the network state over time (Fig. 1a–c). We assume that a subset of N nodes, called drivers, is independently manipulated by external controls and, without loss of generality, we reorder the network nodes such that the N drivers come first. Thus, the network dynamics read as

$$\begin{bmatrix}\dot{\boldsymbol{x}}_{\mathrm{d}}\\ \dot{\boldsymbol{x}}_{\mathrm{nd}}\end{bmatrix}=\begin{bmatrix}A_{11} & A_{12}\\ A_{21} & A_{22}\end{bmatrix}\begin{bmatrix}\boldsymbol{x}_{\mathrm{d}}\\ \boldsymbol{x}_{\mathrm{nd}}\end{bmatrix}+\begin{bmatrix}I_N\\ 0\end{bmatrix}\boldsymbol{u}, \quad (1)$$

where $\boldsymbol{x}_{\mathrm{d}}$ and $\boldsymbol{x}_{\mathrm{nd}}$ are the state vectors of the driver and non-driver nodes, $A_{11}\in\mathbb{R}^{N\times N}$, $M=n-N$, $A_{12}\in\mathbb{R}^{N\times M}$, $A_{21}\in\mathbb{R}^{M\times N}$, $A_{22}\in\mathbb{R}^{M\times M}$, I_N is the N-dimensional identity matrix, and $\boldsymbol{u}$: $\mathbb{R}_{\geq 0}\rightarrow\mathbb{R}^N$ is the control input.

We will use the word *controllable* to refer to networks that are *point-to-point controllable* at time $T\in\mathbb{R}_{\geq 0}$ if, for any pair of states $\boldsymbol{x}_{\mathrm{d}}^*$ and $\boldsymbol{x}_{\mathrm{nd}}^*$, there exists a control input u for the dynamics Eq. (1) such that $\boldsymbol{x}_{\mathrm{d}}(T)=\boldsymbol{x}_{\mathrm{d}}^*$ and $\boldsymbol{x}_{\mathrm{nd}}(T)=\boldsymbol{x}_{\mathrm{nd}}^*$. For a detailed discussion and rigorous conditions for the controllability of a system with linear dynamics, see [30]. We define the energy of $\boldsymbol{u}$ as

$$\mathrm{E}(\boldsymbol{u})=\sum_{i=1}^{N}\underbrace{\int_0^T u_i(t)^2dt}_{\mathrm{E}_i},$$

where u_i is the i-th component of $\boldsymbol{u}$. The energy of u_i can be thought of as a quadratic cost that penalizes large control inputs.

In the context of the brain, we approximate the interactions between brain regions as linear, time invariant dynamics, where a stronger structural connection between two regions represents a stronger dynamic interaction (for empirical motivation, see [23, 31, 32]). We specifically study the empirical inter-areal meso-scale connectomes of the mouse (112 brain regions, example schematic in Fig. 1g, h) from the Allen Brain Institute, the Drosophila (49 brain regions) [29], and a set of human connectomes (116 brain regions) interconnected by

white matter tracts (for empirical details regarding connectivity estimates, see supplementary results XA).

II. PREDICTING CONTROL ENERGY

We seek an accurate, tractable relationship between the energy required to drive a network to a specific state and its connectivity. We begin with the original, *non-simplified network* (Fig. 2a) involving edges between all nodes, and consider dynamics along the *simplified network* (Fig. 2b) involving only edges from the driver to the non-driver nodes (for a conceptual schematic of the full and simplified Drosophila connectome, see Fig. 2c–d). We then derive an approximation of the minimum control energy (Lemma X.2 – X.4) by assuming that $\boldsymbol{x}_{\mathrm{d}}(0) = 0$, $\boldsymbol{x}_{\mathrm{nd}}(0) = 0$ (Assumption 1), and $A_{11} = 0$, $A_{12} = 0$, and $A_{22} = 0$ (Assumption 2) in Eq. (1), which reads as

$$\mathrm{E}(\boldsymbol{u}) = 12(\boldsymbol{x}^*_{\mathrm{nd}} - \frac{1}{2}A_{21}\boldsymbol{x}^*_{\mathrm{d}})^T(A_{21}A_{21}^T)^{-1}(\boldsymbol{x}^*_{\mathrm{nd}} - \frac{1}{2}A_{21}\boldsymbol{x}^*_{\mathrm{d}}) + \boldsymbol{x}^{*T}_{\mathrm{d}}\boldsymbol{x}^*_{\mathrm{d}}. \quad (2)$$

We make Assumption 1 because we are interested in the *change* in brain state through control, and consider initial conditions $\boldsymbol{x}_{\mathrm{d}}(0) = 0$, $\boldsymbol{x}_{\mathrm{nd}}(0) = 0$ to be a neutral baseline. Because Eq. (2) only involves edges from driver to non-driver nodes, we call Eq. (2) a first-order approximation to the minimum control energy of the non-simplified network Eq. (1). Importantly, this approximation requires at least as many driver nodes as non-driver nodes for $A_{21}A_{21}^T$ to be invertible (i.e. $N \geq M$). To assess the accuracy of our expression, we look to classic results in the mathematical theory of systems and control [30], where the spectral properties of the *reachability Gramian* $W_R(0,T) = \int_0^T e^{At}BB^Te^{A^Tt}dt$ quantify the minimum amount of energy (Section XI A 2) to control the non-simplified network Eq. (1).

In these brain networks, we observe that the first-order energy approximation is accurate across a range of parameters, which are the magnitude of the adjacency matrix (given by the magnitude of the largest eigenvalue, $c = \|\lambda_{\max}\|$ after multiplying A by a constant scalar), and the fraction d of nodes selected as non-driver nodes (Fig. 2e–g). The error remains below approximately 5% for scaling $c < 1.5$ and non-driver fraction $d < 0.4$ (Fig. 2e–g). In this paper, we will use these connectomes scaled such that $c = \|\lambda_{\max}\| = 1$, and non-driver fraction $d \leq 0.4$, to ensure generalizability of our findings to the non-simplified versions of these same networks.

III. DETERMINANT OF THE DRIVER-TO-NON-DRIVER NETWORK

After deriving a closed-form approximation for the minimal energy to control a network, we seek a physical interpretation of the mathematical features that predict the control energy. We let $Q = A_{21}A_{21}^T$, and write Eq. (2) as

$$\mathrm{E}(\boldsymbol{u}) = 12\frac{\boldsymbol{v}_1^T\mathrm{adj}(Q)\boldsymbol{v}_1}{\det(Q)} + \boldsymbol{v}_2^T\boldsymbol{v}_2, \quad (3)$$

where $v_1 = x^*_{nd} - \frac{1}{2} A_{21} x^*_d$ and $v_2 = x^*_d$, and adj(Q) is the adjugate matrix of Q. We notice that the determinant of Q acts as a scaling factor for the total energy. This insight is useful because of the geometric interpretation of a Gram matrix determinant. Specifically, let $a_i \in \mathbb{R}^{1 \times N}$ be the i-th row of A_{21} (which we will call the *weight vector*), representing weights from all N drivers to the i-th non-driver node (Fig. 3a). Then, the determinant of the Gram matrix Q is equal to the squared volume of the parallelotope formed by all a_i.

To gain an intuition for these results, we show a simple system with 3 drivers and 2 non-drivers with varying network topologies in Fig. 3b–d, and their corresponding geometric parallelotopes in Fig. 3e–g with weight-vector a_1 in gray and a_2 in tan. We also compute the distribution of control energy required to drive each network from initial states $x_d = 0$, $x_{nd} = 0$ to 10,000 random final states $x^*_{nd} \in (-1,1)^M$, $x^*_d \in (-1,1)^N$ in Fig. 3h. As the non-drivers x_{nd1}, x_{nd2} become more similarly connected, the total area of the parallelotope (and corresponding Gram determinant) decreases (Fig. 3e–g), and the control energy increases (Fig. 3h). We note that this determinant relationship persists for any number of nodes where $N > M$. We conclude that the similarity between weight-vectors generally scales the control energy through det(Q), allowing us to analyze and modify the connectivity of a network with respect to its control energy.

IV. IDENTIFYING ENERGETICALLY FAVORABLE CONTROL NODES

Here, we further explore the idea of "similarity" between connections a_i, to quantify the impact of each individual non-driver on the control energy.

A. Topological contributors to control energy

Our analysis is rooted in the intuition that the edge weights a_i that maximize the parallelotope volume, thereby facilitating network control, are large in magnitude and orthogonal to each other. Let λ_i and e_i be the eigenvalues and eigenvectors of the matrix Q in Eq. (3). We derive in Lemma X.6 the equivalent, alternative control energy expression

$$\mathrm{E}(u) = 12 \left(\frac{\sum_{i=1}^{M} w_i c_i^2}{\sum_{i=1}^{M} w_i} \right) \left(\sum_{k=1}^{M} \frac{1}{\|a_k\|^2 sin(\theta_k)^2} \right) + v_2^T v_2, \quad (4)$$

where $w_i = \prod_{j \neq i}^{M} \lambda_j$, $c_i = e_i^T v_1$, and θ_k is the angle formed between a_k and the parallelotope formed by $a_{j \neq k}$. We also derive in Lemma X.7 the average control energy to reach all random final states drawn uniformly from −1 to 1, $x^*_{nd} \in (-1,1)^M$, $x^*_d \in (-1,1)^N$ as

$$[E(u)] = \frac{1}{3} N + M + 4 \left(\sum_{k=1}^{M} \frac{1}{\|a_k\|^2 sin(\theta_k)^2} \right). \quad (5)$$

For N drivers and M non-drivers, we can visualize the M weight vectors $\boldsymbol{a}_k$ as forming a parallelotope in an N-dimensional space. The variable θ_k then represents the angle formed between a_k and the paralellotope formed by the remaining $M-1$ vectors $\boldsymbol{a}_{j\neq k}$. An example with $N=3$, $M=2$ is shown in Fig. 3e–g, where $\theta_1 = \theta_2$ is the angle between the tan and gray vectors.

Here, we have segregated the control energy into a task-based $\left(\frac{\sum_{i=1}^{M} w_i c_i^2}{\sum_{i=1}^{M} w_i}\right)$ and topology-based $\left(\sum_{k=1}^{M} \frac{1}{\|\boldsymbol{a}_k\|^2 sin(\theta_k)^2}\right)$ term (Eq. 4), where the average minimum control energy depends linearly on the topology-based term (Eq. 5). This segregation allows us to analyze the topology separate from the specific control task, and shows that each non-driver additively contributes to the total control energy minimally when $\|\boldsymbol{a}_i\|$ and $\sin(\theta_i)$ are large.

B. Energetically favorable driver-nondriver sets

To support this discussion, we used expression Eq. (4) to find the selections of M non-drivers that minimized and maximized this topology term (see supplementary results X B), which we define as the *energetically most favorable* and *energetically least favorable* selections, respectively. We show example distributions of each weight-vector's magnitude $\|\boldsymbol{a}_k\|$ times angle $\sin(\theta_k)$ (Fig. 4a–c) between these selections in Drosophila, mouse, and human for non-driver fraction 0.2. We observe that the energetically least favorable selections have significantly weaker magnitudes and angles than the most favorable selections.

Next, we demonstrate the utility and robustness of these topological features for control by computing the minimum control energy along the non-simplified networks using the driver and non-driver designations from the simplified networks in Eq. (4) for a range of non-driver fractions. For each non-driver fraction and species, we computed the control energy to bring the energetically most and least favorable non-driver selections, and 2000 random non-driver selections to a corresponding set of 2000 random final states $\boldsymbol{x}^*_{\mathrm{nd}} \in (-1,1)^M$, $\boldsymbol{x}^*_{\mathrm{d}} \in (-1,1)^N$ (Fig. 4j–l). Across all three species, the most favorable selections require around 0.5–1 order of magnitude less control energy than the random selections, and 2.5–4 orders of magnitude less control energy than the least favorable selections. This difference indicates an energetic advantage for some configurations of drivers and non-drivers over others.

V. COMPLEX BRAIN NETWORKS ARE ENERGETICALLY FAVORABLE

Given the relationship between a network's connectivity and minimum control energy in Eq. (4), we seek to understand if brain networks are organized along energetically favorable principles. Fundamentally, we ask how well a network's specific set of connectivity features $\|\boldsymbol{a}_k\|$ and $\sin(\theta_k)$ combine to minimize the topology-dependent energy term

$\left(\sum_{k=1}^{M} \frac{1}{\|\boldsymbol{a}_k\|^2 sin(\theta_k)^2}\right)$. In networks that are not designed along these energetic principles, we expect to see no particular relationship between $\|\boldsymbol{a}_k\|$ and $\sin(\theta_k)$. In networks that minimize the topology dependent energy term, we expect a compensatory effect, where non-drivers with small angles have large magnitudes, and *vice versa*.

To explore the relationship between $\|\boldsymbol{a}_k\|$ and $\sin(\theta_k)$ in brain networks, we selected 10,000 random permutations of non-drivers in each of the Drosophila, mouse, and 10 human connectomes, at non-driver fraction d. For each permutation, we calculated $\|\boldsymbol{a}_k\|$ and $\sin(\theta_k)$ for every non-driver. Then, we averaged $\|\boldsymbol{a}_k\|$ and $\sin(\theta_k)$ for each non-driver across all permutations, giving us an averaged magnitude $\|\boldsymbol{a}_k\|$ and $\sin(\theta_k)$ for each brain region in each network. Finally, we plotted the averaged $\sin(\theta_k)$ *versus* ka_kk for all brain regions in each network for $d = 0.2$ (Fig. 5a–c). We find little relationship between the averaged $\|\boldsymbol{a}_k\|$ and $\sin(\theta_k)$ in the Drosophila (Spearman $\rho = -0.25$, $p = 0.0748$), a moderate negative relationship in the mouse ($\rho = -0.36$, $p = 0.000125$), and a strong negative relationship in the human ($\rho = -0.73$, $p \approx 0$). This ordering holds for a wide range of non-driver fractions (Fig. 5d). We graphically demonstrate how this negative $\sin(\theta_k)$ *versus* $\|\boldsymbol{a}_k\|$ relation might arise in networks, using a simple 5-node network with two communities of 3 and 2 strongly interconnected sets of nodes (Fig. 5d-f), which has a strong negative relationship (Fig. 5h).

VI. NETWORK MANIPULATION TO FACILITATE CONTROL

Here, we consider network modifications that lead to lower control energies. We focus on the effects of edge deletion since it is often useful in the study of biological systems such as brain [33], metabolic [34], and gene regulatory [35] networks. Specifically, we quantify the effect of modifying each edge weight on the determinant in Lemma X.5 as

$$\frac{\partial}{\partial A_{21}} \det(Q) = 2\det(Q)(Q^{-1}A_{21}), \quad (6)$$

and compute the decrease in control energy as a result of deleting edges that maximally increase the determinant.

First, for each species and each of a range of non-driver fractions, we randomly selected 2,000 permutations of non-drivers. For each permutation, we extracted the block matrix A_{21}, calculated $2\det(Q)(Q^{-1})A_{21}$, and found the element $a_{ij} \neq 0$ yielding the largest increase in $\det(Q)$ based on Eq. (6). We then simulated an edge deletion by setting $a_{ij} = 0$, and repeated the process to obtain networks of 1, 2, 3, and 4 deleted edges. Finally, we computed the percent change in control energy required to bring the non-simplified network from initial states $\boldsymbol{x}_{\mathrm{nd}}(0) = 0$, $\boldsymbol{x}_{\mathrm{d}}(0) = 0$, to final states $\boldsymbol{x}^*_{\mathrm{nd}} \in (-1, 1)^M$, $\boldsymbol{x}^*_{\mathrm{d}} \in (-1, 1)^N$ before and after edge deletion (Fig. 6a–d).

As can be seen in Fig. 6a, the removal of one edge can sometimes lead to more than a 10% average reduction in control energy, while the removal of four edges (Fig. 6d) can

sometimes lead to more than a 30% reduction. Across most non-driver fractions, the Drosophila experienced greater energy reduction than the mouse, which also experienced greater energy reduction than the human. This corresponds to the previous finding where, because brain networks of these increasingly complex species are already energetically favorably wired, they may not experience as much improvement after modification.

VII. CONTRIBUTION AND FUTURE DIRECTIONS

The control of networked systems is a critical frontier in science, mathematics, and engineering, as it requires a fundamental understanding of the mechanisms that drive network dynamics and subsequently offers the knowledge necessary to intervene in real-world systems to better their outcomes [36]. While some theoretical predictions exist in nonlinear network systems [15], the majority of recent advances have been made in the context of linear control [21, 22]. Nevertheless, basic intuitions regarding how edge weights impact control have remained elusive. Although spectral analysis of a network's controllability Gramian [30] yields theoretically useful information about the overall behavior of the network under control [37], it is not obvious how specific patterns of connectivity or selections of driver and non-driver nodes contribute to this behavior. Understanding this relationship is crucial when analyzing empirical biological networks such as the brain, where nodes and edges often have known functions [38] that may modulate or influence one other.

A distinct advantage of our approach is the focus on a physically meaningful topological understanding of the principles governing network control. We map control behavior to network topology through a simplified network only involving connections from driver to non-driver nodes. This simplification hard-codes the fact that energy can be transmitted directly from drivers to non-drivers along walks of length unity, and is motivated by recent work demonstrating that relatively sparse network representations of complex biological systems [39, 40] can contain much of the information needed to understand the system's structure and dynamics [41, 42]. Our results inform our understanding of how much first-order connections contribute to the overall dynamics of our network control systems. Moreover, they inform the development of analytical constraints on the accessible state space of a networked system, particularly informing the set of states within which one might seek to push the brain using stimulation paradigms common in the treatment of neurological disorders and psychiatric disease [43, 44]. While many initial studies have examined unconstrained state spaces [23, 25, 26], understanding viable states and state trajectories is critical for the translation of these ideas into the clinic [45]. Further, by formally quantifying the contribution of the network connectivity to the control energy, we lay the groundwork for the optimization of stimulation sites in neural systems, a problem that has received very little theoretical treatment, and is considered one of the current critical challenges in neuroengineering [46].

Finally, we make strategic, task-agnostic edge deletions that maximally increase the determinant and observe that, even in an overdetermined, unsimplified system ($N > M$), a single edge deletion could produce a profound improvement in the general controllability of a network. This sensitivity suggests that dynamical networks such as the brain can produce

fairly drastic changes in dynamical behavior given minute changes in physiological topology, consistent with observations of critical dynamics in human and animal neurophysiology [47, 48]. Moreover, these results also suggest that minor, targeted structural changes through concussive injury can lead to drastic changes in overall brain function [49, 50], via altering the controllability landscape of the brain [24]. We further observed that these topological modifications were task-agnostic edge deletions, signifying that even in a linear regime, the presence of an unfavorable edge can have a profoundly negative impact on the controllability of a network. We note that it is natural to perform a similar analysis that takes into account the specific tasks $\boldsymbol{v}_1$, $\boldsymbol{v}_2$ by taking the derivative of the full energy term E_{total} with respect to A_{21}, which would optimize the network topology for a specific task, as studied in more detail in [25].

To achieve the most meaningful comparison between species, we only analyzed weighted meso-scale whole brain networks. As such, we did not include binary neuronal connectomes (e.g., *C. elegans*), and binary or partial connectomes (e.g., macaque). As more connectomes become available, we hope to further explore the role of species complexity on network controllability. Until then, we consider the comparison of energetically favorable connectivity between species to be a preliminary excursion into a nuanced evolutionary phenomena. As demonstrated in the significant percent change in energy after edge deletion, we emphasize that uncertainty in network connectivity has the potential to yield substantial changes in average control energy. Finally, we note that while methodological limitations prevent us from resolving excitatory *versus* inhibitory connectivity, all results are directly applicable to networks with signed elements. Further important theoretical considerations and methodological limitations pertinent to our approach, linear model of dynamics, optimality of control trajectories, and empirical data sets are discussed in the SI.

In closing, we note that the natural direction in which to take this work will be to use higher-order approximations of this framework found in the supplement to gain intuition for the role of complex network topologies (e.g. self-loops, cycles) in controlling networks. Moreover, it would be interesting to apply this reduced framework to random graphs and other well-known benchmarks – both from a mathematical perspective [51] and also in the context of neural systems [52, 53] – to better understand the phenotypes present in those graph ensembles. Third and finally, informing the design of new networks with these tools may be particularly useful in neuromorphic computing [54], material science [55], and other contexts where optimal control of physical systems is of paramount importance.

Supplementary Material

Refer to Web version on PubMed Central for supplementary material.

Acknowledgments

JZK acknowledges support from National Institutes of Health T32-EB020087, PD: Felix W. Wehrli, and the National Science Foundation Graduate Research Fellowship No. DGE-1321851. JMS and DSB acknowledge support from the John D. and Catherine T. MacArthur Foundation, the Alfred P. Sloan Foundation, the U.S. Army Research Laboratory and the U.S. Army Research Office through contract numbers W911NF-10-2-0022 and W911NF-14-1-0679, the National Institute of Health (2-R01-DC-009209-11, 1R01HD086888-01, R01-MH107235, R01-MH107703, R01MH109520, 1R01NS099348 R21-M MH-106799, and T32-EB020087), the Office of Naval

Research, and the National Science Foundation (BCS-1441502, CAREER PHY-1554488, BCS-1631550, and CNS-1626008). AEK and JMV acknowledge support from the U.S. Army Research Laboratory contract number W911NF-10-2-0022. FP acknowledges support from the National Science Foundation (BCS-1430280 and BCS 1631112). The content is solely the responsibility of the authors and does not necessarily represent the official views of any of the funding agencies.

References

1. Newman, MEJ. Networks: An Introduction. Oxford University Press; 2010.
2. Newman MEJ. The structure and function of complex networks. SIAM Review. 2003; 45:167–256.
3. Watts DJ, Strogatz SH. Collective dynamics of 'small-world' networks. Nature. 1998; 393:440–2. 0803.0939v1. [PubMed: 9623998]
4. Simon H. The architecture of complexity. Proceedings of the American Philosophical Society. 1962; 10:467–482.
5. Bassett DS, Sporns O. Network neuroscience. Nature Neuroscience. 2016 In Press.
6. Bettencourt LM, Stephens GJ, Ham MI, Gross GW. Functional structure of cortical neuronal networks grown in vitro. Phys Rev E Stat Nonlin Soft Matter Phys. 2007; 75:021915. [PubMed: 17358375]
7. Bassett DS, Bullmore E. Small-world brain networks revisited. Neuroscientist. 2016 In Press.
8. Sporns O, Betzel RF. Modular brain networks. Annu Rev Psychol. 2016; 67:613–640. [PubMed: 26393868]
9. Barabasi AL, Gulbahce N, Loscalzo J. Network medicine: a network-based approach to human disease. Nat Rev Genet. 2011; 12:56–68. [PubMed: 21164525]
10. Ching S, Brown EN, Kramer MA. Distributed control in a mean-field cortical network model: implications for seizure suppression. Phys Rev E Stat Nonlin Soft Matter Phys. 2012; 86:021920. [PubMed: 23005798]
11. Khambhati AN, Davis K, Lucas T, Litt B, Bassett DS. Virtual cortical resection reveals push-pull network control preceding seizure evolution. Neuron. 2016 In Press.
12. Gonen T, et al. Intra-operative multi-site stimulation: Expanding methodology for cortical brain mapping of language functions. PLOS ONE. 2017; 12:e0180740. [PubMed: 28700619]
13. Mohanty SK, Lakshminarayananan V. Optical techniques in optogenetics. Journal of Modern Optics. 2015; 62:949–970. [PubMed: 26412943]
14. Sprott JC, Xiong A. Classifying and quantifying basins of attraction. Chaos. 2015; 25
15. Cornelius SP, Kath WL, Motter AE. Realistic control of network dynamics. Nature communications. 2013; 4:1942. 1307.0015.
16. Shine JM, Koyejo O, Poldrack RA. Temporal metastates are associated with differential patterns of time-resolved connectivity, network topology, and attention. Proc Natl Acad Sci U S A. 2016; 113:9888–9891. [PubMed: 27528672]
17. Mantzaris AV, et al. Dynamic network centrality summarizes learning in the human brain. Journal of Complex Networks. 2013; 1:83–92.
18. Bassett DS, Wymbs NF, Porter MA, Mucha PJ, Grafton ST. Cross-linked structure of network evolution. Chaos. 2014; 24:013112. [PubMed: 24697374]
19. Kalman RE. Mathematical description of linear dynamical systems. J SIAM Control Ser A. 1963; 1:152–192.
20. Lin CT. Structural controllability. IEEE Trans Auto Control. 1974; AC-19:201–208.
21. Liu YY, Slotine JJ, Barabasi AL. Controllability of complex networks. Nature. 2011; 473:167–173. [PubMed: 21562557]
22. Ruths J, Ruths D. Control profiles of complex networks. Science. 2014; 343:1373–1376. [PubMed: 24653036]
23. Gu S, et al. Controllability of structural brain networks. Nature Communications. 2015; 6:8414.
24. Gu S, et al. Optimal trajectories of brain state transitions. Neuroimage. 2017 In Press.

25. Betzel RF, Gu S, Medaglia JD, Pasqualetti F, Bassett DS. Optimally controlling the human connectome: the role of network topology. Scientific Reports. 2016; 6:30770. [PubMed: 27468904]
26. Muldoon SF, et al. Stimulation-based control of dynamic brain networks. PLoS Comp Biol. 2016 In Press.
27. Oh SW, et al. A mesoscale connectome of the mouse brain. Nature. 2014; 508:207–214. [PubMed: 24695228]
28. Rubinov M, Ypma RJ, Watson C, Bullmore ET. Wiring cost and topological participation of the mouse brain connectome. Proc Natl Acad Sci U S A. 2015; 112:10032–10037. [PubMed: 26216962]
29. Shih CT, et al. Connectomics-based analysis of information flow in the Drosophila brain. Current Biology. 2015; 25:1249–1258. [PubMed: 25866397]
30. Kailath, T. Linear Systems. Prentice-Hall; 1980.
31. Fernandez GR. On how network architecture determines the dominant patterns of spontaneous neural activity. PLoS One. 2008; 3:e2148. [PubMed: 18478091]
32. Honey CJ, et al. Predicting human resting-state functional connectivity from structural connectivity. Proc Natl Acad Sci U S A. 2009; 106:2035–2040. [PubMed: 19188601]
33. Alstott J, Breakspear M, Hagmann P, Cammoun L, Sporns O. Modeling the impact of lesions in the human brain. PLoS Computational Biology. 2009; 5
34. Aristidou AA, San KY, Bennett GN. Modification of central metabolic pathway in escherichia coli to reduce acetate accumulation by heterologous expression of the bacillus subtilis acetolactate synthase gene. Biotechnology and Bioengineering. 1994; 44:944–951. [PubMed: 18618912]
35. Sander JD, Joung JK. CRISPR-Cas systems for editing, regulating and targeting genomes. Nature biotechnology. 2014; 32:347–55. NIHMS150003.
36. Motter AE. Networkcontrology. Chaos. 2015; 25:097621. [PubMed: 26428574]
37. Pasqualetti F, Zampieri S, Bullo F. Controllability metrics, limitations and algorithms for complex networks. IEEE Transactions on Control of Network Systems. 2014; 1:40–52.
38. Lanteaume L, et al. Emotion induction after direct intracerebral stimulations of human amygdala. Cerebral Cortex. 2007; 17:1307–1313. [PubMed: 16880223]
39. Park H, Niida A, Miyano S, Imoto S. Sparse overlapping group lasso for integrative multi-omics analysis. J Comput Biol. 2015; 22:73–84. [PubMed: 25629319]
40. Liu Z, Lin S, Deng N, McGovern DP, Piantadosi S. Sparse inverse covariance estimation with l0 penalty for network construction with omics data. J Comput Biol. 2016; 23:192–202. [PubMed: 26828463]
41. Clauset A, Moore C, Newman ME. Hierarchical structure and the prediction of missing links in networks. Nature. 2008; 453:98–101. [PubMed: 18451861]
42. Zhu B, Xia Y. An information-theoretic model for link prediction in complex networks. Sci Rep. 2015; 5:13707. [PubMed: 26335758]
43. Chen HI, et al. Harnessing plasticity for the treatment of neurosurgical disorders: an overview. World Neurosurg. 2014; 82:648–659. [PubMed: 24518888]
44. Chrysikou EG, Hamilton RH. Noninvasive brain stimulation in the treatment of aphasia: exploring interhemispheric relationships and their implications for neurorehabilitation. Restor Neurol Neurosci. 2011; 29:375–394. [PubMed: 22124035]
45. Bassett DS, Khambhati AN, Grafton ST. Emerging frontiers of neuroengineering: A network science of brain connectivity. Annual Reviews in Biomedical Engineering. 2017 Under Consideration.
46. Johnson MD, et al. Neuromodulation for brain disorders: challenges and opportunities. IEEE Trans Biomed Eng. 2013; 60:610–624. [PubMed: 23380851]
47. Rubinov M, Sporns O, Thivierge JP, Breakspear M. Neurobiologically realistic determinants of self-organized criticality in networks of spiking neurons. PLoS Comput Biol. 2011; 7:e1002038. [PubMed: 21673863]
48. Shew WL, et al. Adaptation to sensory input tunes visual cortex to criticality. Nature Physics. 2015; 11:659–663.

49. Caeyenberghs K, Verhelst H, Clemente A, Wilson PH. Mapping the functional connectome in traumatic brain injury: What can graph metrics tell us? . Neuroimage. 2016; S1053-8119:30694–30692.
50. van der Horn HJ, et al. Altered wiring of the human structural connectome in adults with mild traumatic brain injury. J Neurotrauma. 2016 Epub ahead of print.
51. Bollobas, B. Random Graphs. Academic Press; 1985.
52. Klimm F, Bassett DS, Carlson JM, Mucha PJ. Resolving structural variability in network models and the brain. PLoS Comput Biol. 2014; 10:e1003491. [PubMed: 24675546]
53. Sizemore A, Giusti C, Bassett DS. Classification of weighted networks through mesoscale homological features. Journal of Complex Networks. 2016; 4:2016. Published online August.
54. Pfeil T, et al. Six networks on a universal neuromorphic computing substrate. Front Neurosci. 2013; 7:11. [PubMed: 23423583]
55. Giusti C, Papadopoulos L, Owens ET, Daniels KE, Bassett DS. Topological and geometric measurements of force-chain structure. Physical Review E. 2016; 94:032909. 1605.03131. [PubMed: 27739731]

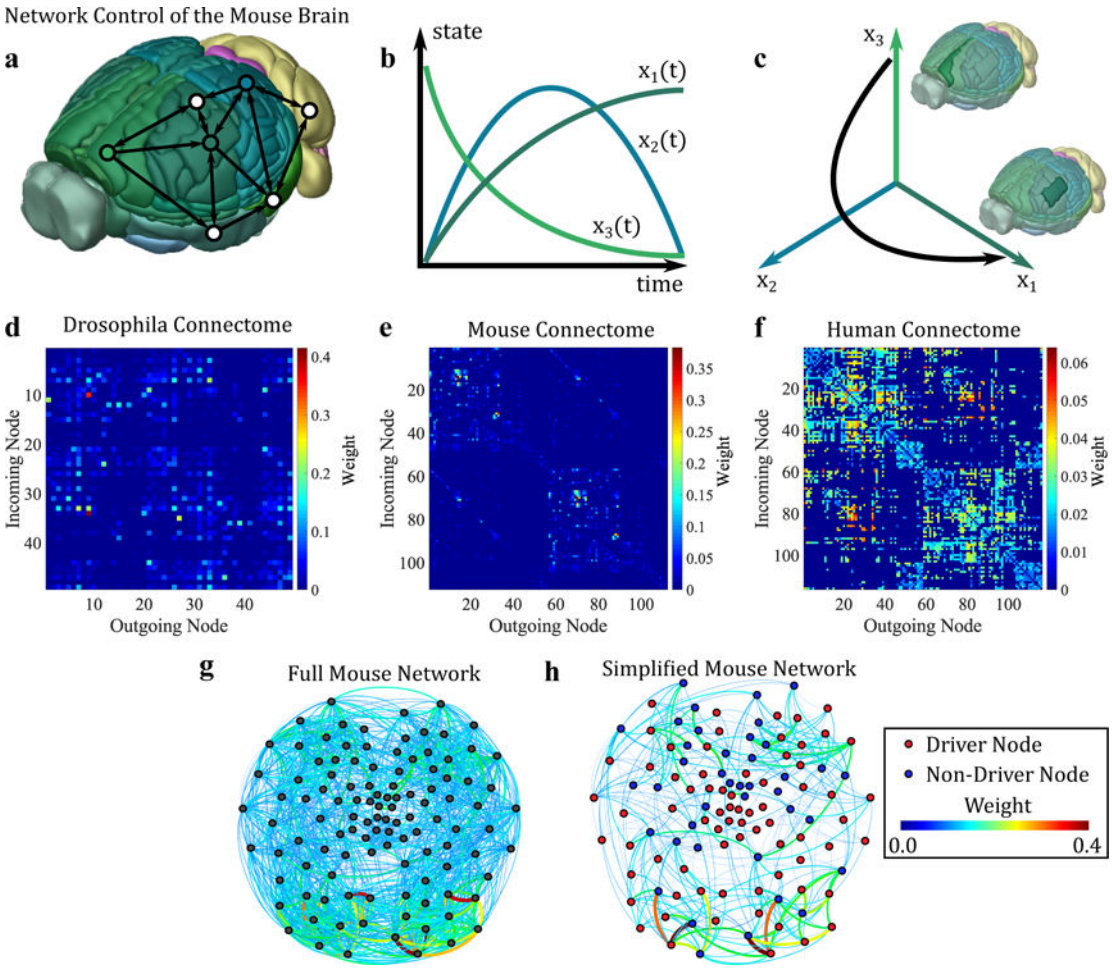

FIG. 1. Network Control of the Drosophila, Mouse, and Human Connectomes

(**a**) A representation of the mouse brain via the Allen Mouse Brain Atlas, with a superimposed simplified network. Each brain region is represented as a vertex, and the connections between regions are represented as directed edges. (**b**) Example trajectories of state over time for three brain regions, where the state represents the level of activity in each region. (**c**) A state-space representation of activity on the mouse connectome over time, where each point on the black line represents the brain state at a point in time. (**d**) Connectomes represented as $n \times n$ adjacency matrices where each i, jth element of the adjacency matrix represents the strength of the connection from node j to node i for Drosophila, (**e**) mouse, and (**f**) human. (**g**) The mouse connectome represented as a graph with vertices as brain regions, and edges colored by their weight, or the magnitude of the relevant element of the adjacency matrix. (**h**) Simplified graph representation: a bipartite subgraph containing edges linking driver vertices (red) to non-driver vertices (blue).

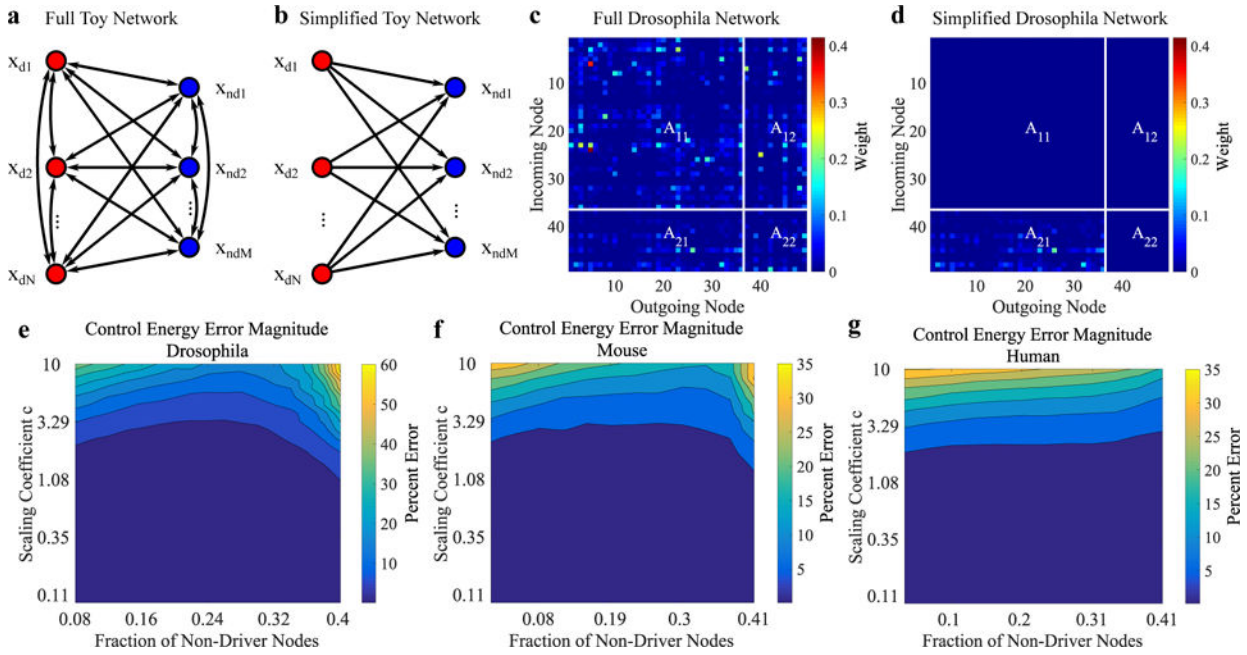

FIG. 2. The Simplified Network Representation Offers a Reasonable Prediction for the Full Network's Control Energy

(**a**) Graphical representation of a *non-simplified* network of N drivers (red) and M non-drivers (blue), with directed connections between all nodes present. (**b**) Graphical representation of a *simplified* first-order network only containing first-order connections from drivers → non-drivers. (**c**) As an example, we show the adjacency matrix for the Drosophila connectome segmented into driver → driver A_{11}, driver → non-driver A_{21}, non-driver → driver A_{12}, and non-driver → non-driver A_{22} sections for a non-simplified network as per Eq. (1), with randomly designated driver and non-driver nodes, and (**d**) the corresponding simplified network as per Eq. (2). (**e**) Percent error contour plots of the total control energy for simplified *versus* non-simplified networks as a function of the fraction of non-driver nodes and matrix scale given by $c = \|\lambda_{\max}\|$. For each combination of parameters, the median error magnitude to drive the networks from initial states $\boldsymbol{x}_{\mathrm{d}} = 0$, $\boldsymbol{x}_{\mathrm{nd}} = 0$ to 1000 random final states $\boldsymbol{x}^*_{\mathrm{nd}} \in (-1,1)^M$, $\boldsymbol{x}^*_{\mathrm{d}} \in (-1,1)^N$ along 1000 corresponding random selections of non-drivers is shown. Each contour represents a 5% interval for the (**e**) Drosophila, (**f**) mouse, and (**g**) human connectome.

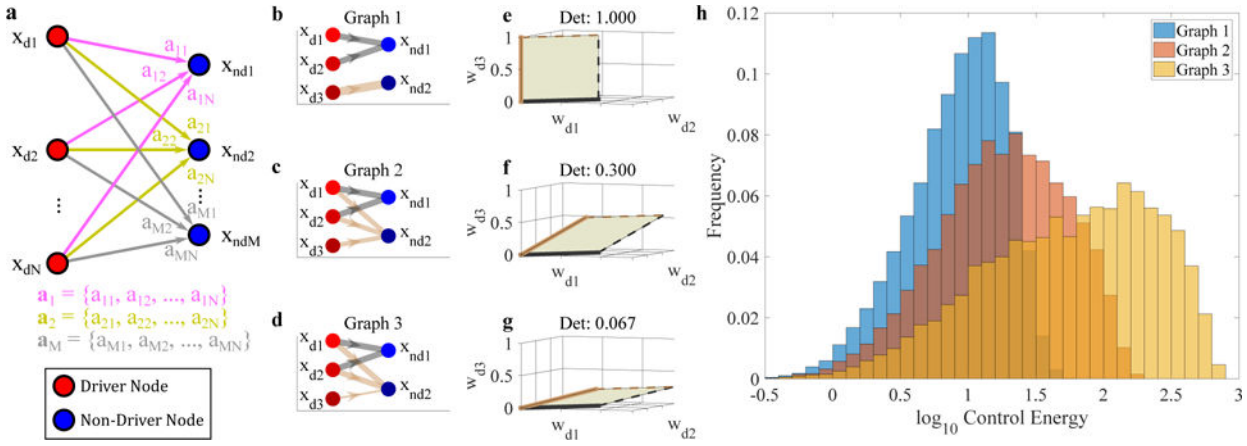

FIG. 3. Geometric Interpretation of Simplified, First-Order Networks with Corresponding Control Energies and Trajectories

(**a**) Graph representation of a simplified first-order network containing connections from N driver nodes in red to M non-driver nodes in blue. The edges connecting all driver nodes to the i-th non-driver corresponding to the i-th row of A_{21} are shown in different colors. (**b**) Graph representation of a network with driver nodes in red, non-driver nodes in blue, weight distribution into non-driver 1 in gray, and weight distribution into non-driver 2 in tan, for dissimilarly distributed weights, (**c**) for somewhat similarly distributed weights, and (**d**) for very similarly distributed weights. (**e**) Geometric representation of the parallelotope formed by the 2 vectors of weight distributions into non-drivers 1 and 2, with the volume shaded in beige for dissimilarly distributed weights, (**f**) for somewhat similarly distributed weights, and (**g**) for very similarly distributed weights. (**h**) Base-10 log distribution of control energy required to bring each graph to 10,000 random final states $\boldsymbol{x}^*_{\mathrm{nd}} \in (-1,1)^M$, $\boldsymbol{x}^*_{\mathrm{d}} \in (-1,1)^N$.

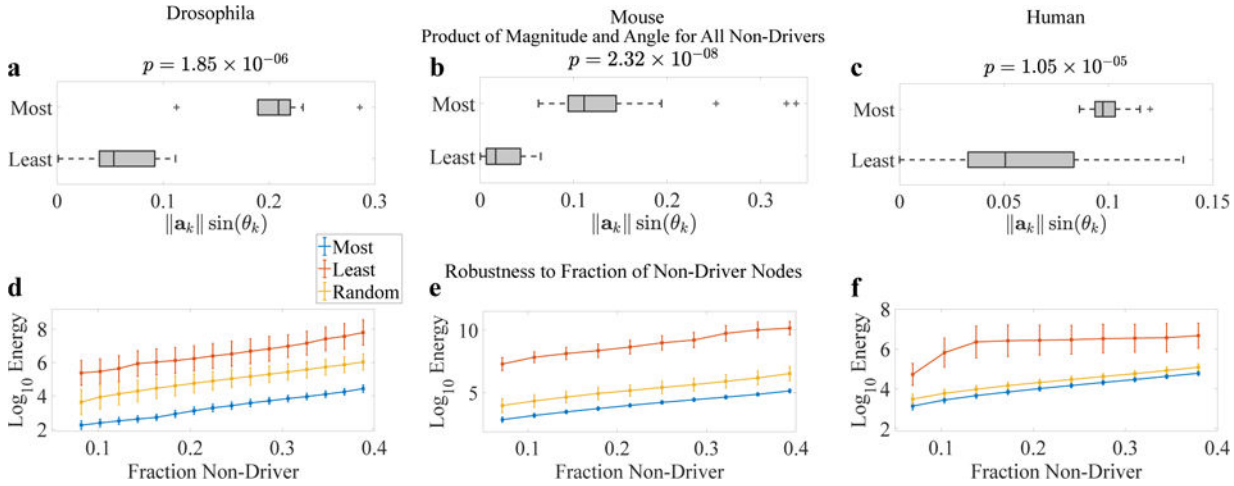

FIG. 4. Topological Characteristics and Energetic Performance of Networks with Energetically Favorable and Unfavorable Topologies

(**a**) Boxplot of each non-driver weight-vector's magnitude and angle product ($\| \boldsymbol{a}_k \| \sin(\theta_k)$) between the energetically most and least favorable networks in the Drosophila, (**b**) mouse, and (**c**) human connectomes, for a non-driver fraction of 0.2 and *p*-values from a 2-sample *t*-test. (**d**) Mean and standard deviations of the base-10 log of the minimum control energies required to bring the system to 2000 random final states $\boldsymbol{x}^*_{\mathrm{nd}} \in (-1,1)^M$, $\boldsymbol{x}^*_{\mathrm{d}} \in (-1,1)^N$ for each of a range of non-driver fractions for the energetically most favorable, least favorable, and random networks for the Drosophila, (**e**) mouse, and (**f**) human.

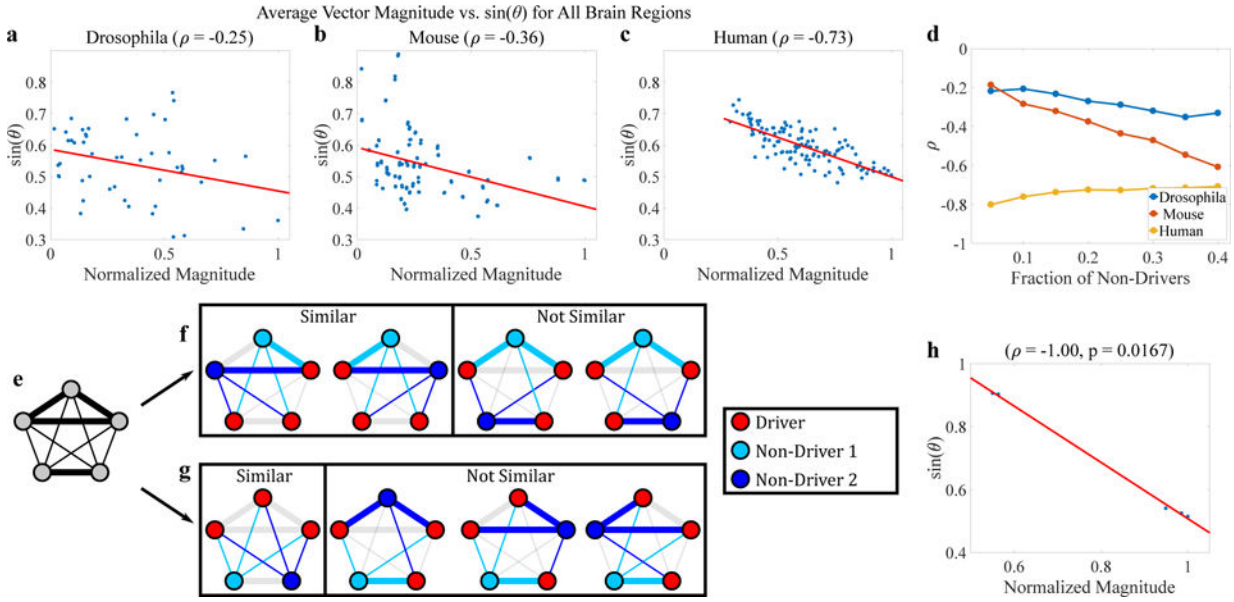

FIG. 5. Energetically Favorable Organization of Topological Features in Networks

(**a**) Average $\sin(\theta_k)$ *versus* normalized $\|\boldsymbol{a}_k\|$ for each brain region across 10,000 random non-driver selections for a non-driver fraction of 0.2, along with best fit line (red) and corresponding Spearman correlation coefficient in the Drosophila, (**b**) mouse, and (**c**) human. (**d**) Spearman correlation coefficients in the Drosophila, mouse, and human over 2,000 random non-driver selections for each of a range of non-driver fractions. (**e**) Example toy network of 5 nodes with three strongly interconnected nodes at the top, and two strongly interconnected nodes at the bottom. (**f**) Representation of similarity in driver → non-driver connections between Non-Driver 1 (light blue, member of three strongly connected nodes) and all possible selections of Non-Driver 2 (blue). Across all 4 configurations, Non-Driver 1 has an average of 1.5 strong connections, and 2/4 similarly connected (small angle) configurations. (g) Similarity in driver → non-driver connections between Non-Driver 1 (light blue, member of two strongly connected nodes) and all selections of Non-Driver 2 (blue). Across all 4 configurations, Non-Driver 1 has an average of 0.75 strong connections, and 1/4 similarly connected configurations. (**h**) Plot of average magnitude *versus* $\sin(\theta)$ for the toy network, with Spearman rank correlation coefficient.

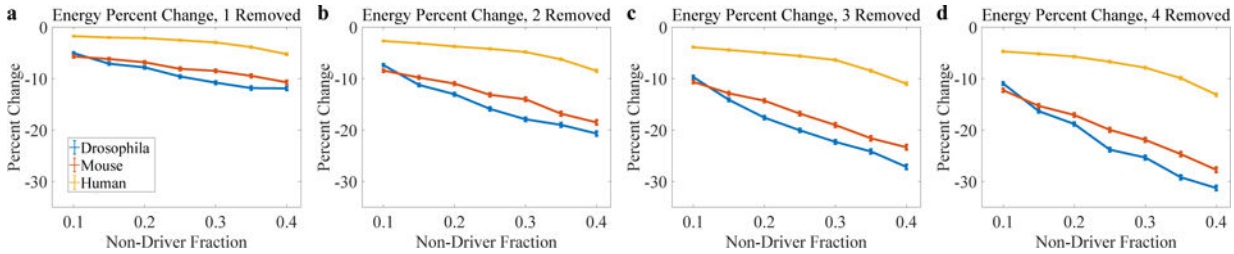

FIG. 6. Modifying the Drosophila, Mouse, and Human Connectomes to Decrease the Minimum Energy Required for Control

(**a**) Means and standard errors of percent change in control energy before and after deleting edges that maximally increase the determinant based on Eq. (6) over 2,000 control tasks, with initial states $x_{\mathrm{nd}}(0) = 0$, $x_{\mathrm{d}}(0) = 0$, and random final states $\boldsymbol{x}^*_{\mathrm{nd}} \in (-1, 1)^M$, $\boldsymbol{x}^*_{\mathrm{d}} \in (-1, 1)^N$. Non-drivers were randomly selected for a range of non-driver fractions in the Drosophila, mouse, and human connectomes for 1 deletion, (b) 2 deletions, (**c**) 3 deletions, and (**d**) 4 deletions. Standard errors were computed as $SE = \frac{s}{\sqrt{n}}$, where s is the sample standard deviation over the 2,000 tasks, and $n = 2,000$.